MULTIFUNCTIONAL THERMOPLASTIC ELASTOMER NANOCOMPOSITES REINFORCED BY GRAPHENE

Mufeng Liu[1], Dimitrios G. Papageorgiou[1], Ian A. Kinloch[1], Robert J. Young[1]

[1]National Graphene Institute, School of Materials, The University of Manchester, Oxford Rd, Manchester, M13 9PL, UK
Email: mufeng.liu@postgrad.manchester.ac.uk,WebPage: https://advancednanomaterials.weebly.com/phd-students.html
Email: dimitrios.papageorgiou@manchester.ac.uk,WebPage: https://advancednanomaterials.weebly.com/pdras.html
Email: ian.kinloch@manchester.ac.uk, Web Page: https://advancednanomaterials.weebly.com/prof-ian-a-kinloch.html
Email: robert.young@manchester.ac.uk, Web Page: https://advancednanomaterials.weebly.com/prof-robert-j-young.html

Keywords: elastomer, nanocomposites, graphene, micromechanics

Abstract
In this work, a series of graphene-reinforced thermoplastic elastomers were prepared, with the introduction of graphene nanoplatelets (GNPs) of different particle diameter. Their microstructures were characterised by SEM and quantified by polarised Raman spectroscopy. It was shown that the GNPs were well-dispersed and their orientation across the cross-section of the injection moulded samples was consistent with the shear rate profile of fountain flow mechanism. The mechanical properties of the nanocomposites were evaluated by tensile testing and it was found that the GNPs contributed to significant improvements in both the stiffness and strength of the TPE. A micromechanical model based on the combination of shear-lag theory and the rule-of-mixtures, which was developed specifically for polymer nanocomposites reinforced by nanoplatelets, was introduced to analyse the stiffening mechanisms. It was found that the effective aspect ratio of GNPs was in the order of 100 and decreases with the increasing filler loading due to agglomeration. Finally, the stress transfer efficiency from the matrix to GNPs was evaluated by observing the Raman band shifts under tension and the effective modulus of the nanoplatelets was also calculated.

1. Introduction

Thermoplastic elastomers (TPEs) based on thermoplastic vulcanizate blends are considered an interesting class of materials since they combine the melt processability of thermoplastics with the properties of conventional thermoset rubbers [1]. The TPEs usually have excellent weatherability, ozone resistance, chemical resistance to oils and abrasion resistance; however, their applications are limited by their relatively poor mechanical properties [2]. In this context, inorganic fillers have been incorporated within the TPEs and enhancements in their mechanical performances have been reported in the literature [3-7]. More recently, since the isolation of monolayer graphene [8] and the discovery of its unique properties, graphene and graphene-related nanomaterials have been employed extensively as reinforcement in elastomers [9].

In the present work, we have undertaken a comprehensive study of the mechanisms of reinforcement of a TPE by GNPs. The composite samples based on a commercially-available TPE (Alcryn®) and GNPs with three different flake sizes were prepared by melt mixing. The microstructure of the injection moulded specimen was studied by quantifying the orientation factor of the fillers with polarised Raman spectroscopy. The mechanical properties of the nanocomposites with different filler loadings were evaluated by tensile testing followed by stress transfer measurements by observing the 2D Raman band shifts of the fillers during *in situ* deformation. Moreover, we applied our recently developed theory [10] to the experimental results from tensile testing and correlated the fittings with

important geometrical characteristics of the filler, such as the effective aspect ratio. Through the experimental and theoretical analysis, we can conclude that the enhancement of thermoplastic elastomers with graphene nanoplatelets is effective, and gives considerable potential to develop high-performance engineering plastics, with tuned, application-specific properties.

2. Experimental Methods

2.1. Materials and preparation

Graphene nanoplatelets (GNPs) with nominal lateral diameters of 5, 10, 25 μm (dimensions claimed by the supplier) and average thicknesses in the range of 6-8 nanometres were purchased from XG Sciences, Inc. Lansing, Michigan, USA and used as received. Three grades of xGnP® M5, M15 and M25 were used. The thermoplastic elastomer, Alcryn® 2265 UT (Unfilled Translucent), which is based on a partially crosslinked chlorinated olefin interpolymer alloy, was purchased from A. Schulman, Inc. The melt mixing of the composites was undertaken in a Thermo Fisher HAAKE Rheomix internal mixer. The mixing took place at 165 oC and 50 rpm for 5 minutes. The GNP fractions in the nanocomposites were 1%, 5%, 10%, and 20% by weight. The Alcryn nanocomposites in this study are coded based on the type of the matrix, the diameter and weight content of the fillers. For example, the sample code 2265-M15-GNP10, means that the matrix is the Alcryn 2265, the diameter of the GNPs is 15 μm and the weight percentage of the filler is 10 wt%. The dumbbell-shaped tensile specimens were prepared by injection moulding in a HAAKE Minijet Piston Injection Moulding System. The temperatures of the barrel and the mould were set as 185 oC and 30 oC. The injection pressures were 500 bar, 550 bar, 600 bar, 700 bar and 800 bar for the neat polymer and the nanocomposites filled with 1 wt%, 5 wt%, 10 wt% and 20 wt% of GNPs, respectively. The injection pressure was held for 10 seconds followed by post-injection pressure of 200 bar, held for 5 seconds, for all specimens.

2.2. Characterization of the nanocomposites

The actual loadings of GNPs in the nanocomposites were obtained by thermogravimetric analysis (TGA) using a TA Q500 TGA instrument. The samples were heated from room temperature up to 600 oC under a 50 mL/min flow of N_2 at 10 ^oC/min. Three samples were tested for each material in order to ensure reproducibility of the results. The morphologies of the fillers, neat polymer and the microstructure of the nanocomposites were examined using scanning electron microscopy (SEM). The images were acquired using a high-resolution XL30 Field Emission Gun Scanning Electron Microscope (FEGSEM) at 6 kV. The XRD diffractograms were obtained from a PANalytical X'Pert3 diffractometer with Cu Kα radiation. The 2-theta angle range was selected from 5° to 90° with a step size of 0.03o and a step time of 180 s operated at 40 kV and 40 mA. Stress–strain curves were obtained using dumbbell-shaped specimens in an Instron 4301 machine, under a tensile rate of 50 $mm \cdot min^{-1}$ with a load cell of 5 kN. Raman spectra were obtained using a Renishaw InVia Raman spectrometer with a laser wavelength of 633 nm and an objective of ×50, which produces a spot size of 1-2 μm. The Raman 2D band shift of the injection moulded samples (gauge length ~ 55 mm) was studied following the application of strain on the nanocomposites with the highest loading of GNPs (20 wt%). The tests were carried out using a mini-tensile rig. The strain was determined by measuring the extension of the two grips with a digital caliper. The Raman laser spot was in the order of 1-2 μm and it was focused on the same point of a single flake on each sample surface. The results were based on 5 composite samples for each type of GNPs, at the highest loading. All the spectra were fitted with a single Lorentzian curve. The spatial orientation of the GNPs in the composites was determined using the method reported in previous studies from our group [11, 12]. The equipment employed was a 514 nm Raman spectrometer by Renishaw with 'VV' (vertical-vertical) polarisation, in which the incident and scattered radiation were polarised in the same direction.

3. Results and discussion

3.1. Characterisation of the filler and matrix

The three types of GNPs were examined by scanning electron microscopy as shown in Figs. 1(a-c). It can be seen that the flake size increases from M5 to M15 to M25. However, the M15 and M25 GNPs batches seem to include a number of smaller flakes, which may decrease their average lateral size. Another important observation is that folded and looped structures can be found particularly in larger flake samples (Fig .1 d and e). Overall, the three types of fillers display the stacked and agglomerated structure of many-layer graphene. The cryo-fractured cross-section of the neat elastomer can be also seen in Fig. 1(f). Two distinct morphologies can be observed, revealing the two components in the matrix and indicating that the polymer blend is not completely miscible, as expected from earlier reports [1].

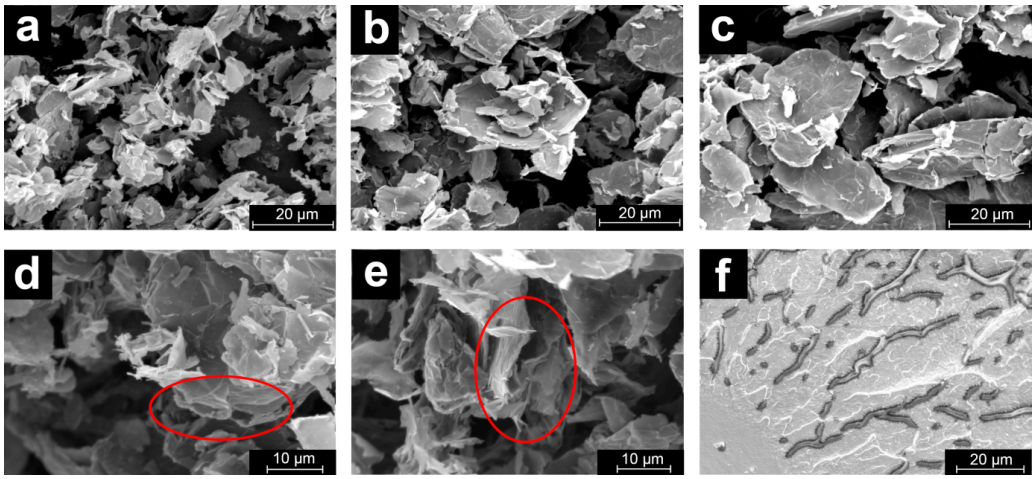

Figure 1. SEM images of (a-c) M5, M15 and M25 GNP powders, (d,e) M15 and M25 GNPs showing folded or looped structure and (f) neat elastomer.

The Raman spectra of the GNPs are shown in the Fig. 2(a). The G (~1580 cm^{-1}) and 2D bands (~2680 cm^{-1}) are well defined for all types of the nanoplatelets, consistent with the signature of graphitic structures. The 2D bands are broad and asymmetric suggesting that the nanoplatelets consist of many layers of graphene [11, 21, 22]. Moreover, broad and weak D bands can be observed at ~ 1360 cm^{-1} which is an indication of defects that are present in the structure. The XRD patterns of GNPs are also shown in Fig. 2(b), which display the sharp and strong peaks at $2\theta \approx 26°$ consistent with reflections from the (002) plane of graphite, while weak peaks can be seen at $2\theta \approx 42.1$, 44.3 and 54.4° corresponding to reflections from (100), (010) and (004) planes, respectively.

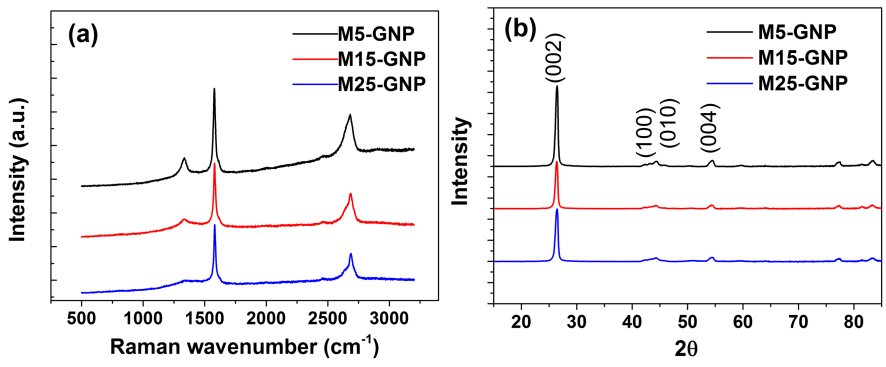

Figure 2. (a) Raman spectra and (b) XRD patterns of M5, M15 and M25 GNPs.

3.2. Characterisation of the composites

The cross-sectional surfaces of cryo-fractured dumbbell samples were investigated by SEM as shown in Figs. 3. The low magnification images of the composites with highest loading (20 wt%) Figs. 3 (a-c) indicate that a uniform distribution of the fillers was achieved even at high filler contents. The observation of different regions of the cross-section, reveals a distinct alignment of the fillers, which was induced by the shear rate distribution during the injection moulding procedure, known as a fountain flow mechanism. There are regions within the samples with different degrees of orientation of the fillers, due to the variation of shear rate generated by the combination of the injection pressure and the slightly lower temperature of the mould walls. The high magnification SEM images (Figs. 3 d-f) demonstrate the morphologies of the individual flakes within the matrix. Generally, the interface between the matrix and the nanoplatelets is intact, without voids or gaps, which is expected to contribute to higher reinforcement efficiency. Interestingly, the shorter flakes tend to maintain their shape after processing, as shown in Fig.3 (d), while on the other hand, the larger ones can be seen bent or form looped-folded morphologies as shown in Figs.3 (e, f). It can be also seen that the flakes tend to restack and form agglomerates, particularly at higher loadings, which will reduce the reinforcing efficiency.

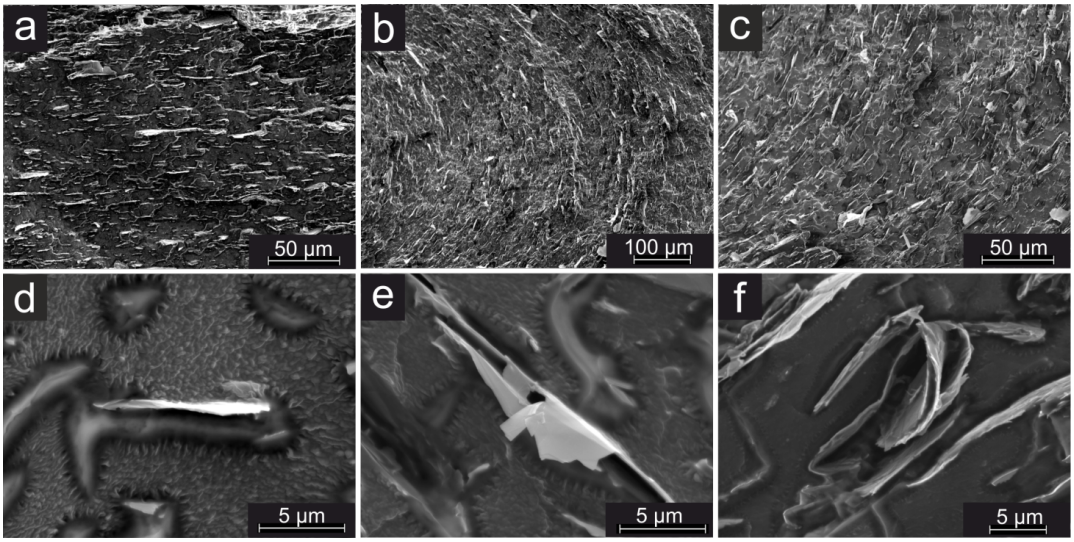

Figure 3. SEM images of cryo-fractured cross-section of the injection moulded composites: (a-c) low magnification images of the composites (2265-M5-GNP20) showing preferred orientation of the flakes in accordance with fountain flow mechanism; (e-f) High magnification images of M5, M15 and M25 GNPs in the composites showing the interface between the filler and the matrix and preferred morphologies dependent on the sizes of the fillers.

Since it is obvious from SEM that the flakes have a preferred alignment, it is possible to quantify the orientation factor using polarised Raman spectroscopy [12]. Different regions across the cryo-fractured cross-sections of the samples were studied by using a rotation stage. From the results shown in Figs. 4, it can be seen that when the laser is polarised parallel to the Z axis, there is no change in G band intensity with the rotation of Φ_Z, indicating no preferred orientation. In contrast, the G band intensity decreases from 0° to 90° and subsequently increases from 90° to 180° when the sample is rotated around the X axis, which is an indication that the flakes tend to be oriented along the X axis. The calculated average orientation factor can be used to evaluate the effect of orientation on the reinforcing efficiency of the filler [12]. The $\langle P_2(\cos\theta)\rangle$ and $\langle P_4(\cos\theta)\rangle$ values described in detail in Refs. [11, 12] are obtained by the X axis tests along with the curve fitting using equation (1).

$$I_{sample}(\Phi)=I_0\left\{\frac{8}{15}+\langle P_2(\cos\theta)\rangle\left(-\frac{16}{21}+\frac{8}{7}\cos^2\Phi\right)+\langle P_4(\cos\theta)\rangle\left(\frac{8}{35}-\frac{8}{7}\cos^2\Phi+\cos^4\Phi\right)\right\} \quad (1)$$

where I_o is the amplitude and assuming the surface normals are uniformly distributed around the Z-axis.

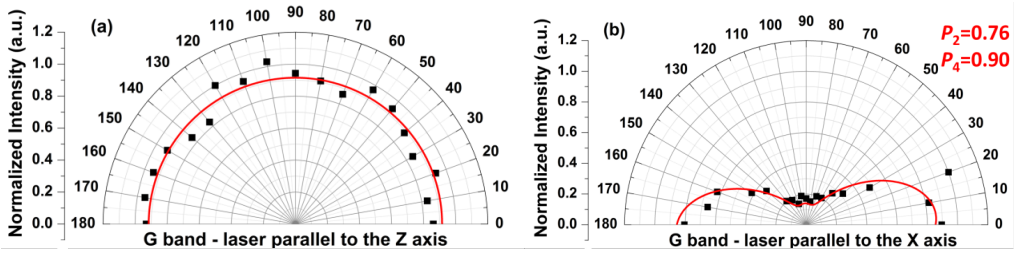

Figure 4. Representative fitting of normalized G band intensities parallel to the (a) Z and (b) X axis as a function of rotational angle for M5 GNPs.

Subsequently, the orientation factor η_o is given by:

$$\eta_o = \frac{8}{15} + \frac{8}{21}\langle P_2(\cos\theta)\rangle + \frac{3}{35}\langle P_4(\cos\theta)\rangle \quad (2)$$

In this experiment, the calculated average orientation factors are 0.76, 0.69 and 0.62 for M5, M15, and M25, respectively. The orientation factor values clearly imply that the degree of orientation decreases with increasing flake size, due to looped and folded morphologies of the larger diameter flakes, which is in agreement with the results reported by Li et al. on GNP-reinforced natural rubbers [11].

3.3 Mechanical properties

Tensile testing was used to evaluate the mechanical properties of the materials. The stress-strain behaviour of all injection moulded samples is presented in Fig. 5(a). It can be seen that the addition of GNPs up to ~10 vol% increases the stiffness and tensile strength of the thermoplastic elastomer significantly. Overall, larger flakes are more efficient in increasing the modulus, whereas the smaller flakes contribute to better tensile strength enhancements. It is also apparent that the addition of GNPs results in a reduction of strain at failure. The initial Young's modulus values are plotted against the volume fractions of the fillers in Fig. 5(b). As expected, in all cases, the modulus increases significantly with increasing GNP content. The modulus values of the composites are up to ~6 times higher (at 20 wt% filler loading) compared with the matrix, indicating the stiffening effect of the fillers. The reinforcement mechanism of graphene in composites is attributed to the interfacial stress transfer from the matrix to the flakes; larger platelets resulting in larger aspect ratio are beneficial for stress transfer on the basis of the well-established shear-lag theory [13, 14]. Tensile strength and strain at failure values are also plotted against GNP volume fractions in Figs. 5(c-d). The tensile strength increases with increasing GNP loading, indicating a strong interaction between the fillers and the matrix. It has been reported that the wrinkled structure of graphene flakes can improve the tensile strength by acting as a crack propagation barrier and improve the mechanical interlocking between the matrix and the filler [15]. It can be clearly seen that the tensile strength enhancement is dependent significantly upon the flake size, particularly at high filler loadings. Tensile strength is known to depend heavily on the dispersion characteristics [16]; therefore these results indicate higher degree of aggregation of larger flakes at higher loadings and looped/folded flake morphologies similar to the ones seen in Fig. 3(e,f). The strain at failure declines significantly with increasing filler fraction. Similar results have been observed not only for elastomeric nanocomposites but almost all polymer nanocomposites where agglomerated fillers act as failure points during elongation [9]. The effect of the addition of GNPs upon the stiffness of the elastomer can be evaluated by an equation we recently developed, which is the result of the simultaneous use of the rule-of-mixtures along with the well-accepted shear-lag theory [10]. The modulus of the composite is given by:

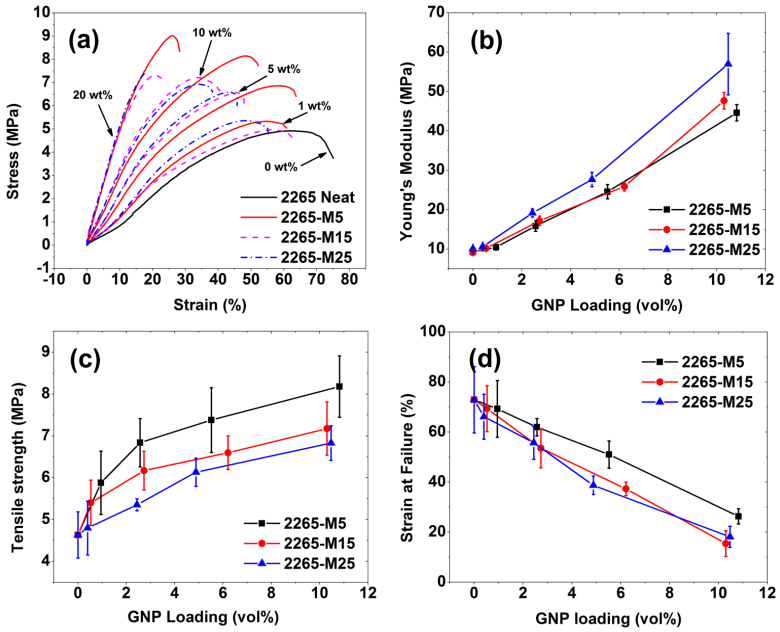

Figure 5. (a) Stress-strain curves of the materials; (b-d) Plots of the values of stiffness, tensile strength and strain at failure against volume fractions of the GNPs.

$$E_c \approx E_m\left(1-V_f+\frac{s^2}{12}\frac{\eta_o}{(1+\nu)}V_f^2\right) \quad (3)$$

where V_f is the volume fraction of the filler, E_m and E_f are the Young's Modulus of the matrix and the filler, respectively; s is the aspect ratio of the filler in the composites; η_o is the orientation factor of the GNPs and ν is the Poisson's ratio of the matrix. Equation (3) reveals that for soft materials the composite modulus is only dependent on V_f and s^2 and independent of the filler modulus (E_m<500 MPa) [10]. This fact allows us to focus on the effective aspect ratio s_{eff} of the reinforcement, since the formation of agglomerates and the bending/folding of the flakes during processing affects the nanoplatelets critically. The results of the fitting of the experimental data with the above equation can be seen in Figs. 6(a-c). The reason for the relatively small values of aspect ratio can be attributed to the restacking and agglomeration of the flakes that is unavoidable, especially at higher filler loading and to the additional presence of looped and folded flakes in the composites, that can preexist in the batches of the nanoplatelets or can also originate from the shear forces applied to the flakes during melt mixing/injection moulding. As shown in Fig. 3(f), the looped/folded flakes can even form hollow structures, resulting in significant reductions of the aspect ratio values.

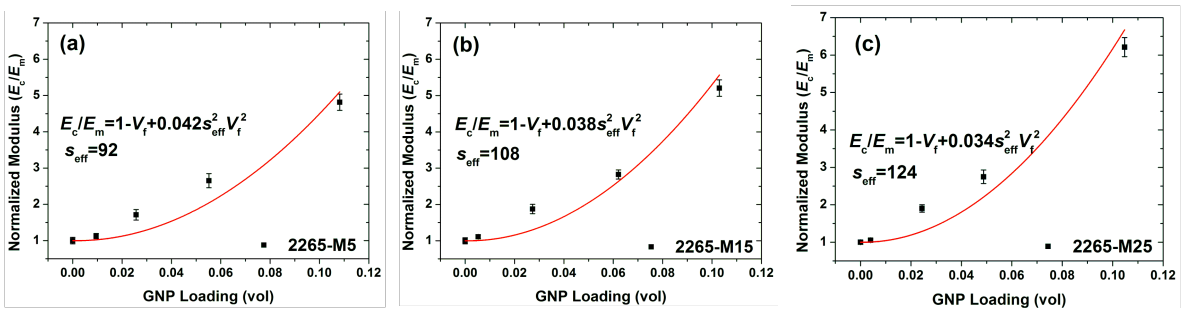

Figure 6. Normalized Young's Modulus against the volume fraction of the filler and fitted data using equation (3) for (a) 2265-M5, (b) 2265-M15 and (c) 2265-M25 samples.

3.4 Stress-induced 2D Raman band shifts

The samples with the highest amount of filler (20 wt%) were strained in situ under a Raman spectrometer and the characteristic shifts of the Raman bands were recorded with increasing strain. The slope of the band shifts at different strain levels represents the stress transfer efficiency between the matrix and the filler [10]. For each composite reinforced by M5, M15 and M25 nanoplatelets, 5 samples were tested, in order to give the average values shown in Fig. 7. It was shown that the flakes display very low 2D band shifts, with obvious scattering on the linear curve fitting, indicating the significantly lower stress transfer efficiency of this elastomeric material than the stiffer matrices of previous studies [10] but higher than softer matrices such as natural rubber [13]. The small values of the slope indicate the low effective modulus of GNPs within the TPE matrix, compared with pristine graphene (-60 cm^{-1}/% strain for the 2D band that corresponds to a modulus of 1050 GPa) [14, 17]. This is because the interfacial stress transfer efficiency in graphene nanocomposites depends upon the stiffness of the matrix (the effective modulus of graphene increases with increasing stiffness of the matrix), as discussed in our previous study [10].

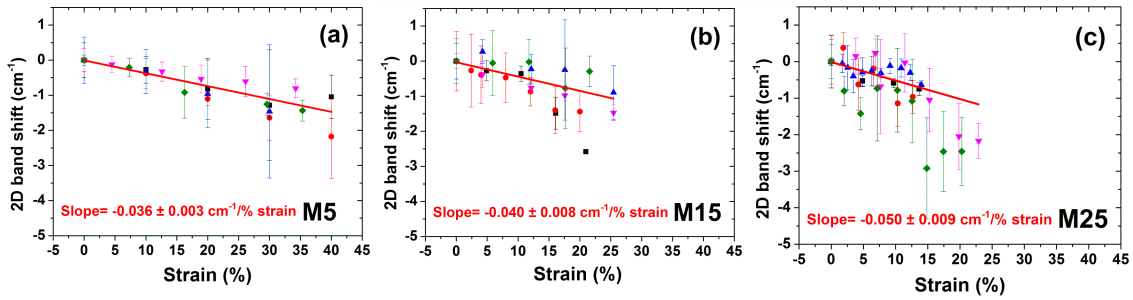

Figure 7. 2D Raman band shifts of (a-c) M5, M15 and M25 flakes respectively against the composite strain. Different colours represent different sets of measurements. The fittings were carried out based on all measurements for each type of GNP.

In our previous work, we showed that on the basis of the shear-lag theory, for soft matrices reinforced by graphene nanoplatelets, the Young's modulus of the flakes obtained from Raman experiments (E_R) is higher than the filler modulus (E_f) acquired from tensile testing [10]. The Raman modulus of the graphene flakes is given by:

$$E_R = -\frac{d\omega_{2D}}{d\varepsilon}\frac{1050}{-60}\text{GPa} \quad (4)$$

where $-d\omega_{2D}/d\varepsilon$ is the 2D Raman band shift rate per % composite strain for any type of graphene.

Table 1. Raman 2D band shift and corresponding modulus values calculated using Eq. (4).

	M5	M15	M25
Band shift (cm^{-1}/% strain)	-0.036 ± 0.003	-0.040 ± 0.005	-0.050 ± 0.006
E_R (MPa)	630 ± 53	700 ± 88	875 ± 105

4. Conclusion

It can be concluded that the reinforcement efficiency of the GNPs on a thermoplastic elastomer matrix is highly dependent on the filler geometry and also the processing method. The improvements of the stiffness and strength, to a large extent, rely on the effective aspect ratio of the flakes. The processing method, on the other hand, affects the dispersion, orientation and further intercalation of the filler significantly, which is of a great significance in determining the filler geometry in the bulk

nanocomposites. The composites produced show great promise in terms of their mechanical properties and can be considered as high-performance engineering plastics that can be attractive to a number of high-tech industries such as automobile or aerospace, as well as their possible use in conventional consumer goods.

References

[1] Akkapeddi M. Commercial polymer blends. Polymer blends handbook: Springer; 2003. p. 1023-1115.
[2] Drobny JG. Handbook of thermoplastic elastomers: Elsevier; 2014.
[3] Costa P, Silva J, Sencadas V, Simoes R, Viana J, Lanceros-Méndez S. Mechanical, electrical and electro-mechanical properties of thermoplastic elastomer styrene–butadiene–styrene/multiwall carbon nanotubes composites. Journal of Materials Science. 2013;48(3):1172-1179.
[4] Frogley MD, Ravich D, Wagner HD. Mechanical properties of carbon nanoparticle-reinforced elastomers. Composites Science and technology. 2003;63(11):1647-1654.
[5] Katbab A, Nazockdast H, Bazgir S. Carbon black-reinforced dynamically cured EPDM/PP thermoplastic elastomers. I. Morphology, rheology, and dynamic mechanical properties. Journal of applied polymer science. 2000;75(9):1127-1137.
[6] Khan U, May P, O'Neill A, Coleman JN. Development of stiff, strong, yet tough composites by the addition of solvent exfoliated graphene to polyurethane. Carbon. 2010;48(14):4035-4041.
[7] Koerner H, Price G, Pearce NA, Alexander M, Vaia RA. Remotely actuated polymer nanocomposites—stress-recovery of carbon-nanotube-filled thermoplastic elastomers. Nature materials. 2004;3(2):115-120.
[8] Novoselov KS, Geim AK, Morozov SV, Jiang D, Zhang Y, Dubonos SV, et al. Electric field effect in atomically thin carbon films. science. 2004;306(5696):666-669.
[9] Papageorgiou DG, Kinloch IA, Young RJ. Graphene/elastomer nanocomposites. Carbon. 2015;95:460-484.
[10] Young RJ, Liu M, Kinloch IA, Li S, Zhao X, Vallés C, et al. The mechanics of reinforcement of polymers by graphene nanoplatelets. Composites Science and Technology. 2018;154:110-116.
[11] Li S, Li Z, Burnett TL, Slater TJ, Hashimoto T, Young RJ. Nanocomposites of graphene nanoplatelets in natural rubber: microstructure and mechanisms of reinforcement. Journal of Materials Science. 2017;52(16):9558-9572.
[12] Li Z, Young RJ, Wilson NR, Kinloch IA, Vallés C, Li Z. Effect of the orientation of graphene-based nanoplatelets upon the Young's modulus of nanocomposites. Composites Science and Technology. 2016;123:125-133.
[13] Cox H. The elasticity and strength of paper and other fibrous materials. British Journal of Applied Physics. 1952;3(3):72.
[14] Gong L, Kinloch IA, Young RJ, Riaz I, Jalil R, Novoselov KS. Interfacial stress transfer in a graphene monolayer nanocomposite. Advanced Materials. 2010;22(24):2694-2697.
[15] Wakabayashi K, Pierre C, Dikin DA, Ruoff RS, Ramanathan T, Brinson LC, et al. Polymer−Graphite Nanocomposites: Effective Dispersion and Major Property Enhancement via Solid-State Shear Pulverization. Macromolecules. 2008;41(6):1905-1908.
[16] Papageorgiou DG, Kinloch IA, Young RJ. Mechanical properties of graphene and graphene-based nanocomposites. Progress in Materials Science. 2017;90:75-127.
[17] Lee C, Wei X, Kysar JW, Hone J. Measurement of the elastic properties and intrinsic strength of monolayer graphene. science. 2008;321(5887):385-388.